第 40 卷 第 2 期
2019 年 2 月
焊 接 学 报
TRANSACTIONS OF THE CHINA WELDING INSTITUTION
Vol. 40(2):077 − 081
February 2019

基于最小二乘支持向量机的激光拼焊焊缝识别

邹媛媛[1,2], 左克铸[1,2], 房灵申[3], 李鹏飞[1,2]

(1. 沈阳建筑大学 机械工程学院, 沈阳 110168; 2. 高档石材数控加工装备与技术国家地方联合工程实验室, 沈阳 110168; 3. 中国科学院 沈阳自动化研究所, 沈阳 110016)

摘 要: 激光拼焊焊缝质量结构光视觉检测中, 对焊缝的准确识别是实现高精度检测的关键. 针对检测图像中结构光光纹畸变特征不明显, 无法准确识别焊缝的问题, 依据焊缝纹理特征信息, 提出了一种基于最小二乘支持向量机的焊缝识别方法. 首先, 分析并提取焊缝区和非焊缝区差异明显的纹理特征. 其次, 训练最小二乘支持向量机模型, 对焊缝进行粗识别. 最后, 采用 Laws 纹理滤波提取焊缝区域, 并通过阈值分割方法精确识别焊缝. 针对不同工艺参数下的激光拼焊焊缝开展焊缝识别试验, 结果表明, 该方法能够有效地识别焊缝.

关键词: 焊缝识别; 图像分割; 最小二乘支持向量机; 激光拼焊

中图分类号: TG 409 **文献标识码:** A **doi:** 10. 12073/j. hjxb. 2019400046

0 序 言

激光拼焊作为一种先进的焊接技术, 在航空航天、汽车等工业领域有着广泛应用[1-2]. 焊接过程中, 焊缝质量检测是实现焊接自动化的关键技术之一[3], 目前多采用结构光视觉传感器采集焊缝图像[4], 通过阈值法[5]、边缘检测法[6] 等图像分割方法提取结构光光纹信息, 并基于结构光光纹畸变点识别焊缝, 进而检测焊缝质量. 其中, 对焊缝区域的准确识别是实现高精度焊缝质量检测的关键.

与其它焊接形式不同, 激光拼焊焊缝具有焊缝窄、变形小等特点[7], 尤其当检测的激光拼焊板板厚差较小或是板厚相等时, 结构光畸变特征不明显, 无法准确识别焊缝区域. 因此, 仅依据结构光信息识别焊缝具有一定的局限性. 由于焊缝灰度图像除了包括结构光特征外, 还包括纹理特征, 焊缝区域的纹理特征对比其它区域有显著的不同, 因此, 通过提取图像中纹理特征对焊缝区域进行识别, 能够解决结构光畸变不明显情况下焊缝的测量问题. 然而, 在实际生产中, 焊缝图像信息具有不确定性, 焊缝存在油烟污染、热影响区不规则等现象, 需要焊缝识别算法具有一定的适应性.

收稿日期: 2017 − 09 − 12

基金项目: 国家自然科学基金资助项目 (51405481); 辽宁省教育厅科研资助项目 (LJZ2016016); 江苏省产学研合作项目 (BY2015063-01); 沈阳建筑大学学科涵育计划资助项目 (XKHY2-32)

支持向量机 (support vector machine, SVM) 是一种无监督式学习分类方法, 学习泛化能力很强, 因此被广泛应用于图像分割领域[8]. 其中, 最小二乘支持向量机 (least square support vector machine, LSSVM) 是一种改进的支持向量机模型, 提高了支持向量机求解的速度和精度[9].

文中提出一种基于最小二乘支持向量机的激光拼焊焊缝识别方法, 该方法通过分析并提取焊缝区和非焊缝区差异明显的纹理特征, 对焊缝识别采用两级识别方法. 首先, 通过样本数据训练最小二乘支持向量机模型, 对焊缝进行粗识别. 其次, 对粗识别得到的焊缝图像, 采用纹理滤波和阈值法精确识别焊缝. 该识别方法识别精度高, 适应性强, 能够有助于实现激光拼焊焊缝质量自动检测.

1 最小二乘支持向量机图像分割原理

最小二乘支持向量机是一种改进的支持向量机模型, 将标准 SVM 的线性不等式约束转化成等式约束, 将误差的二范数作为优化目标的损失函数, 使 SVM 的训练等价于一组线性方程组的求解[9]. 给定一个训练样本集

$$S = \{s_i | s_i = (x_i, y_i), x_i \in R^n, y_i \in (-1, +1)\}_{i=1}^{l} \quad (1)$$

式中: x_i 是第 i 个输入样本; y_i 是第 i 个样本的类标.

LSSVM 在优化目标中选取误差ξ_i的平方项作为允许错分的松弛变量, 相当于求解下式最小值.

$$\min J(\omega,\xi)=\frac{1}{2}\omega'\omega+\frac{1}{2}C\sum_{i=1}^{l}\xi_i^2 \tag{2}$$

$$s.t.\ \ y_i[\omega'\varphi(x_i)+b]=1-\xi_i, i=1,2,\cdots,l$$

为求解这个问题，会引入拉格朗日函数，得到LSSVM的最优分类函数为

$$y(x)=sgn\left[\sum_{i=1}^{l}a_i y_i k(x,x_i)+b\right] \tag{3}$$

式中：$k(x,x_i)$为核函数；sgn为符号函数.

文中LSSVM图像分割原理是利用LSSVM模型对每一个图像子块进行分类. 首先，将图像划分若干图像子块，通过提取分别代表两类的各图像子块的特征信息，生成训练集，训练得到LSSVM模型，其次，提取待分类的图像子块特征信息，生成待分类样本集，依据上述公式计算每一个图像子块样本到超平面的距离，最后，将每一个图像子块归入到对应的类，实现图像分割.

2 焊缝纹理特征分析与提取

激光拼焊板一般包括母材区、热影响区和焊缝区三部分，如图1所示，拼焊板三部分区域纹理各不相同，母材区具有一般金属的纹理特征，热影响区较为平滑，而焊缝区由于焊接过程熔融状态下金属的流动，具有重复出现的且有一定结构性和方向性的纹理. 对于自然纹理采用统计法比较适用[10]，因此，文中采用统计值来表征焊缝纹理信息，包括基于灰度直方图统计特征值和基于灰度共生矩阵的统计特征值.

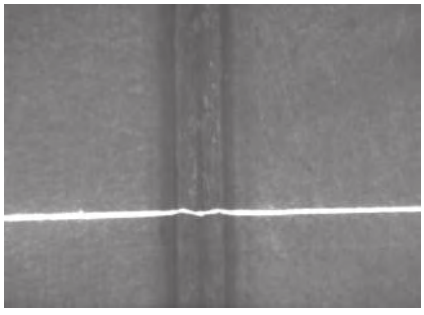

图1 激光拼焊焊缝图像

Fig. 1 Weld seam image of tailored blanks

基于灰度直方图进行统计特征的计算，可以提供纹理的粗糙、平滑和规则等性质的统计量. 设一个图像区域大小为$M\times N$，L为该区域的灰度级数. z_i是表示亮度的随机变量，$p(z_i)$是该区域的灰度概率分布，则灰度均值的第n阶矩定义为

$$\mu_n=\sum_{i=0}^{L-1}(z_i-m)^n p(z_i) \tag{4}$$

式中：$m=\sum_{i=0}^{L-1}z_i p(z_i)$.

二阶矩即图像方差σ^2，是灰度对比度的度量，标准偏差σ是平均对比度度量. 三阶矩可以用来衡量直方图倾斜度. 平滑度表示区域中亮度的相对平滑度度量. 熵是表示随机性度量. 平滑度、熵、一致性分别定义为

$$R=1-1/(1+\sigma^2) \tag{5}$$

$$e=-\sum_{i=0}^{L-1}p(z_i)\log_2 p(z_i) \tag{6}$$

$$U=\sum_{i=0}^{L-1}p^2(z_i) \tag{7}$$

在图1中母材区、热影响区及焊缝区各取一块子图，计算基于灰度直方图的统计特征值，如表1所示.

表1 基于灰度直方图的纹理度量

Table 1 Texture measurements based on gray histogram

区域	均值	标准偏差	三阶矩	平滑度	熵	一致性
母材区	105.160 0	5.451 3	0.000 0	0.000 4	4.453 6	0.051 4
热影响区	74.506 0	4.733 3	0.000 2	0.000 3	4.242 3	0.058 4
焊缝区	94.080 0	7.719 5	0.003 2	0.000 9	4.901 0	0.038 8

统计结果表明焊缝区纹理粗糙，其均值、标准偏差和三阶矩相比母材区和热影响区均具有较大差异. 然而仅基于灰度直方图的统计特征没有考虑到像素的位置信息，这里引入灰度共生矩阵，它是像素对的联合分布矩阵，能够反映图像灰度在某一方向和间隔的综合信息[11]，其中，$p(z_i, z_j)$表示图像f中灰度值z_i和z_j在距离d和方向θ成对出现的概率，对所有的灰度级进行统计计算得出结果，其中L为图像的灰度级. 常用的基于灰度共生矩阵的特征量有能量V_1、对比度V_2、同质性V_3、熵V_4、相关V_5和最大概率V_6，分别定义为

$$V_1=\sum_{i=0}^{L-1}\sum_{j=0}^{L-1}[p(z_i,z_j)]^2 \tag{8}$$

$$V_2=\sum_{i=0}^{L-1}\sum_{j=0}^{L-1}(z_i-z_j)^2 p(z_i,z_j) \tag{9}$$

$$V_3=\sum_{i=0}^{L-1}\sum_{j=0}^{L-1}\frac{p(z_i,z_j)}{1+|z_i-z_j|} \tag{10}$$

$$V_4=-\sum_{i=0}^{L-1}\sum_{j=0}^{L-1}p(z_i,z_j)\times\log_2 p(z_i,z_j) \tag{11}$$

$$V_5=\sum_{i=0}^{L-1}\sum_{j=0}^{L-1}\frac{(z_i-m_r)(z_j-m_c)p(z_i,z_j)}{\sigma_r\sigma_c} \tag{12}$$

$$V_6=\max(p(z_i,z_j)) \tag{13}$$

式中: $m_r=\sum_{i=0}^{L-1}z_i\sum_{j=0}^{L-1}p(z_i,z_j)$; $\sigma_r^2=\sum_{i=0}^{L-1}(z_i-m_r)^2\sum_{j=0}^{L-1}p(z_i,z_j)$; $m_c=\sum_{i=0}^{L-1}z_j\sum_{j=0}^{L-1}p(z_i,z_j)$; $\sigma_c^2=\sum_{i=0}^{L-1}(z_j-m_c)^2\sum_{j=0}^{L-1}p(z_i,z_j)$.

由于考虑到焊缝为垂直方向, 所以选取方向 $\theta=90^\circ$. 分别计算在不同步长情况下各区域的灰度共生矩阵, 并统计上述 6 个特征值, 如图 2 所示, 图中横坐标为步长 d, 纵坐标为各特征值. 通过对比分析可以发现, 当方向一定时, 特征值大小随步长的变化而变化, 当步长较小时, 一些特征值差别较小, 难以有效的区分不同区域, 因此 d 不宜取值太小. 其中对比度、能量和熵等指标, 焊缝区相比母材区和热影响区均具有较大差异.

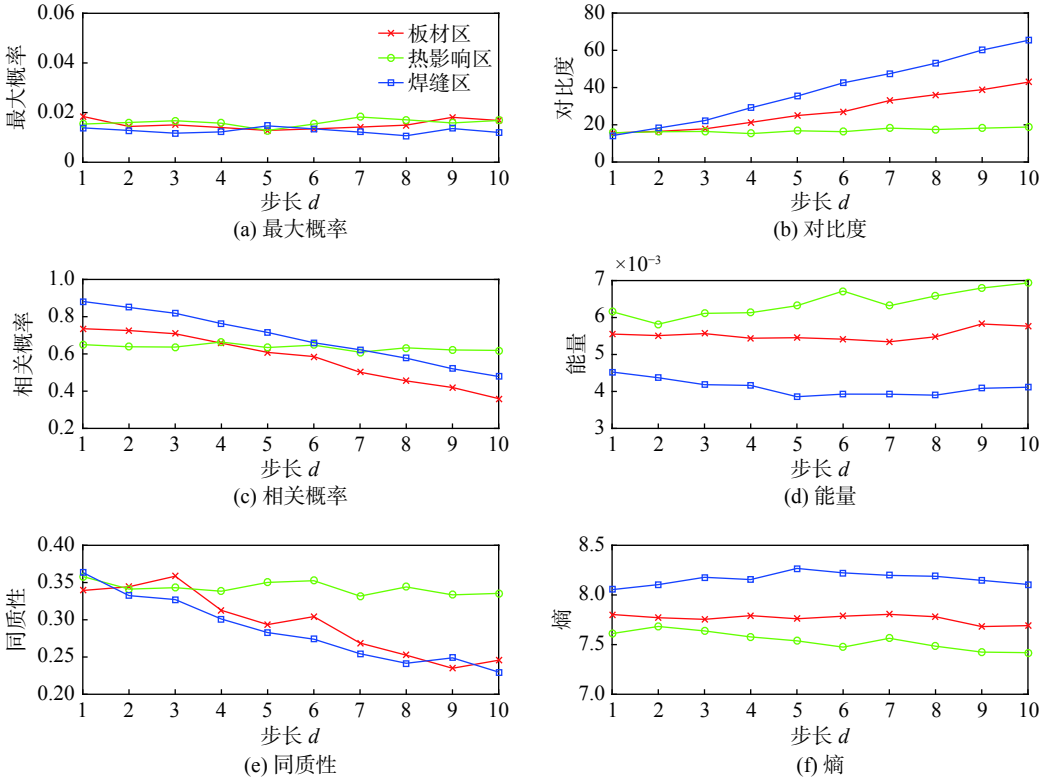

图 2　不同步长下灰度共生矩阵特征值

Fig. 2　Eigenvalue of GLCM in different steps

3　焊缝识别算法

焊缝质量检测中, 当检测图像中结构光畸变特征不明显时, 一般的图像分割方法很难将焊缝区域准确地分割识别出来. 采用两级识别方法. 首先, 基于焊缝区域的纹理特征, 采用最小二乘支持向量机学习分类方法, 实现对焊缝区域粗分割. 其次, 通过纹理滤波方法精确识别焊缝区域. 具体的步骤如下. (1) 对拼焊焊缝图像提取感兴趣区域. 仅讨论焊缝纹理特征, 因此, 感兴趣区域不包括结构光光纹部分; (2) 将感兴趣区域图像划分成 n 个图像子块, 通过试验确定焊缝图像子块尺寸, 图像子块应该尽可能小, 且能够包括焊缝纹理信息, 对图像子块进行标记, 并计算其纹理特征值; (3) 分析并提取焊缝区和非焊缝区差异明显的纹理特征; (4) 依据获取的样本数据训练得到焊缝区域分割的最小二乘支持向量机模型; (5) 采用训练好的模型对焊缝图像进行分割, 获得焊缝粗分割结果; (6) 对分割得到的结果进行后处理, 通过保留最大连通区域, 并填充孔洞来消除误判区域; (7) 处理后的图像采用 Laws 纹理滤波提取焊缝区域, 并通过均值滤波对图像进行平滑处理, 抑制图像噪声; (8) 对滤波后的图像采用阈值分割法准确识别焊缝区域.

4 试验结果与分析

根据上述的焊缝分割识别方法，对拼焊焊缝进行识别试验. 对焊缝图像做行方向上和列方向上的灰度累加投影，依据灰度投影曲线的局部极值设定感兴趣窗口，提取感兴趣区域图像. 通过试验确定图像子块尺寸为 20 pixel × 20 pixel，并通过试验对比分析确定灰度共生矩阵的生长步长为 10. 计算每个图像子块的特征向量，特征向量由基于灰度直方图的统计度量，分别为均值、标准差、三阶矩，以及基于灰度共生矩阵的纹理度量，分别为对比度、能量、熵共 6 个特征组成，对样本特征进行归一化处理后，训练 LSSVM，其中选用径向基函数作为核函数.

使用训练好的 LSSVM 对焊缝图像进行分割识别，并对识别分类后的图像进行后续处理，仅保留最大连通区域，即焊缝所在区域，对被焊缝子块包围但被判别为非焊缝的子块进行填充，去除区域边缘突出的子块、填充凹陷的子块等，初步确定焊缝区域. 采用 Laws 纹理能量法中的$\boldsymbol{L}_5'\boldsymbol{E}_5$模板[12] 对焊缝图像进行滤波，该模板与图像进行卷积操作可以凸显焊缝区，其中，$\boldsymbol{L}_5'\boldsymbol{E}_5$可以由列向量$\boldsymbol{L}_5'$与行向量$\boldsymbol{E}_5$相乘得到，即

$$\boldsymbol{L}_5' = [1\ \ 4\ \ 6\ \ 4\ \ 1]' \tag{14}$$

$$\boldsymbol{E}_5 = [-1\ \ -2\ \ 0\ \ 2\ \ 1] \tag{15}$$

经过 Laws 滤波处理后，焊缝的纹理得到增强，但仍存在大量的噪声干扰，使用均值滤波器对图像进行平滑，抑制噪声. 最终，使用阈值分割方法对滤波后图像进行分割，得到焊缝区域的精确识别，并提取焊缝左右边缘，焊缝图像处理与识别结果分别如图 3 所示.

针对不同工艺参数下的拼焊焊缝正面和背面图像训练 LSSVM，使用训练好的 LSSVM 对拼焊焊缝进行焊缝识别试验，工艺参数如表 2 所示，图 4 为试验装置，包括激光拼焊装备、焊缝质量检测传感器和焊缝图像处理系统等. 识别结果如图 5 所示.

试验结果表明，提出的方法可以有效进行焊缝的提取，能够实现焊缝区域的准确识别. 识别过程中，识别的准确性主要与采集焊缝图像中纹理特征是否显著、最小二乘支持向量机模型参数选择等因素有关，可以通过提高采集图像质量，优化模型参数来保证.

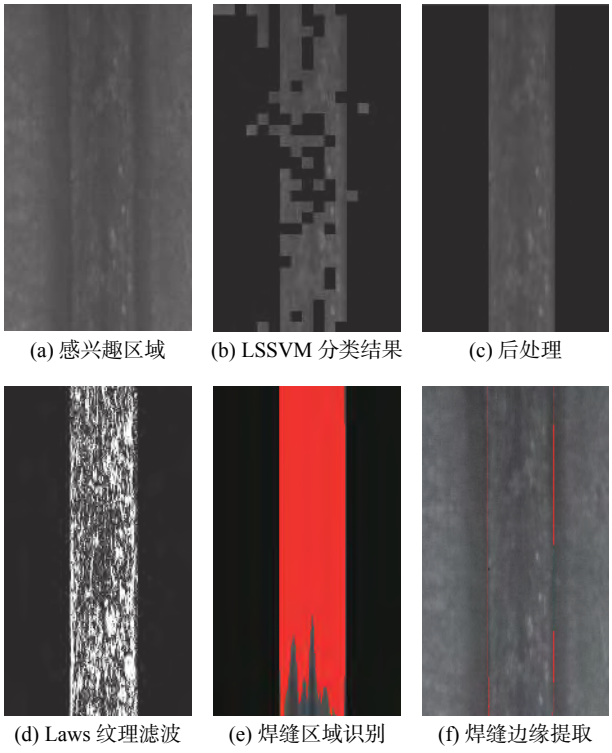

图 3 焊缝识别图像处理结果

Fig. 3 Image processing results of weld seam recognition

表 2 焊接工艺参数

Table 2 Welding parameters

序号	板厚(厚−薄)d/mm	焊接功率P/kW	焊接速度v/(mm·min^{-1})
第一组	1.4−1.8	3.5	6.5
第二组	1.4−1.8	3.5	6.5
第三组	0.6−1.0	2	3

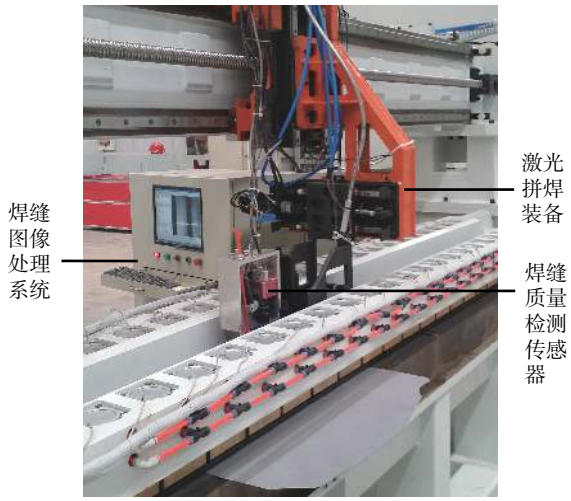

图 4 激光拼焊焊缝识别试验装置

Fig. 4 Experimental equipment for weld seam recognition

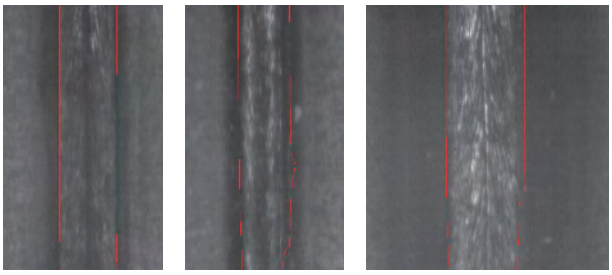

(a) 第一组背面焊缝　(b) 第二组正面焊缝　(c) 第三组背面焊缝

图 5　焊缝识别结果

Fig. 5　Results of weld seam recognition

5　结　　论

(1) 分别基于灰度直方图和灰度共生矩阵的纹理特征表征方法分析了激光拼焊焊缝的纹理特征, 选择了能够凸显激光拼焊焊缝的纹理特征.

(2) 依据焊缝纹理特征信息, 给出了一种基于最小二乘支持向量机的激光拼焊焊缝识别方法, 首先, 通过训练最小二乘支持向量机模型, 对焊缝进行粗识别, 其次, 采用 Laws 纹理滤波提取焊缝区域, 并通过阈值分割方法精确识别焊缝.

(3) 针对不同工艺参数下的激光拼焊焊缝开展焊缝识别试验, 试验结果表明, 文中提出的焊缝识别方法识别精度高, 适应性强, 能够有效进行焊缝识别.

参考文献:

[1] Irving B. Welding tailored blanks is hot issue for automakers[J]. Welding Journal, 1995, 74(8): 49 − 52.

[2] 夏卫生, 刘　奋, 韦春华, 等. 激光拼焊板 HAZ 力学性能的预测及有限元分析 [J]. 焊接学报, 2016, 37(3): 79 − 82.
Xia Weisheng, Liu Fen, Wei Chunhua, *et al*. Prediction and finite element analysis of the mechanical properties of heat affected zone of laser welded blanks[J]. Transactions of the China Welding Institution, 2016, 37(3): 79 − 82.

[3] Chen Yanbin, Tao Wang, Li Liqun, *et al*. Visual sensing and morphological image processing of weld pool in laser spot welding[J]. China Welding, 2010, 19(2): 70 − 74.

[4] Nguyen H C, Lee B R. Laser-vision-based quality inspection system for small-bead laser welding[J]. International Journal of Precision Engineering and Manufacturing, 2014, 15(3): 415 − 423.

[5] 伏喜斌, 林三宝, 杨春利, 等. 基于激光视觉传感的角焊缝外形尺寸检测 [J]. 焊接学报, 2008, 29(7): 47 − 50.
Fu Xibin, Lin Sanbao, Yang Chunli, *et al*. Inspection of fillet weld shape dimension based on laser vision sensing[J]. Transactions of the China Welding Institution, 2008, 29(7): 47 − 50.

[6] Xu M, Zhao M Y, Zhang C N. Image processing method for weld quality inspection system of tailored blanks laser welding[C]// 2010 International Conference on Measuring Technology and Mechatronics Automation. Changsha 2010: 422–426.

[7] 王平江, 吴家勇, 陈吉红, 等. 激光焊接中狭窄对接拼缝测量方法 [J]. 中国机械工程, 2010, 21(17): 2132 − 2137.
Wang Pingjiang, Wu Jiayong, Chen Jihong, *et al*. A method for measuring seam topograph in tailored blank laser welding[J]. China Mechanical Engineering, 2010, 21(17): 2132 − 2137.

[8] Park S, Lee HS, Kim J. Seed growing for interactive image segmentation using SVM classification with geodesic distance[J]. Electronics Letters, 2017, 53(1): 22 − 23.

[9] 宋召青, 程子君, 郑　苏, 等. 基于平滑滤波与最小二乘支持向量机的指纹图像识别研究 [J]. 海军航空工程学院学报, 2010, 25(2): 172 − 176, 180.
Song Zhaoqing, Cheng Zijun, Zheng Su, *et al*. Research on the fingerprint image recognition based on smooth filter and least square support vector machine[J]. Journal of Naval Aeronautical and Astronautical University, 2010, 25(2): 172 − 176, 180.

[10] 王胜华, 都　东, 曾　凯, 等. 基于纹理特征的焊缝识别方法 [J]. 焊接学报, 2008, 29(11): 5 − 8.
Wang Shenghua, Du Dong, Zeng Kai, *et al*. Weld recognition based on texture feature[J]. Transactions of the China Welding Institution, 2008, 29(11): 5 − 8.

[11] 陈　英, 杨丰玉, 符　祥. 基于支持向量机和灰度共生矩阵的纹理图像分割方法 [J]. 传感器与微系统, 2012, 31(9): 60 − 63.
Chen Ying, Yang Fengyu, Fu Xiang. Method of texture image segmentation based on SVM and gray level co-occurrence matrix[J]. Transducer and Microsystem Technologies, 2012, 31(9): 60 − 63.

[12] Laws K I. Textured image segmentation[D]. University of Southern California, 1980.

第一作者简介: 邹媛媛, 女, 1981 年出生, 博士, 副教授, 硕士研究生导师. 主要从事焊缝跟踪与质量检测方面的科研工作. 发表论文 20 余篇. Email: yyzou@sjzu.edu.cn

Cu interlayer. There are obvious indentations on the surface of NiTi welding due to the effect of sonotrode tip. Well bonding could be observed at the weld interface, and no intermetallic compound was formed. Ultrasonic welding NiTi shape memory alloy showed a reversible phase transition process. The strength of NiTi memory alloy joints reached 65% of the base material, and the fracture surface showed ductile fracture characteristic. Ultrasonic welding method conlat solve the problem of brittle intermetallic compounds produced by traditional fusion welding method, which provides a new solution for the connection of NiTi shape memory alloys.

Key words: shape memory alloy; ultrasonic welding; weld morphology; mechanical properties

Analysis of beam scattering and weld morphology in helium protected by ultra-low vacuum electron beam welding CHEN Jian, LENG Bing, ZHENG Hong, SU Jinhua (Harbin Welding Institute Limited Company, Harbin 150028, China). pp 68-72

Abstract: In order to solve the problems of melting depth and melting width reduction, and unstable welding process caused by severe scattering of electron beam in low vacuum and local vacuum electron beam welding. The variation of electron beam and weld morphology with the acceleration voltage of 100 kV, beam current of 60 mA and vacuum of 133.32 ~ 1 333.2 Pa was studied. A coaxial helium shielded welding process is proposed. During the welding of low carbon steel, the whole process is stable. The weld penetration is 30 ~ 40 mm, and the electron beam welding joint with large aspect ratio is obtained.

Key words: electron beam; beam scattering; ultra-low vacuum; helium protection

Effect of surfactant on TC4 sheet with back reflection induced synergistic laser welding WANG Hongyu[1], DING Rui[1], CHAO Shuan[2], LI Le[1] (1. School of Mechanical Engineering, Jiangsu University, Zhenjiang 212013, China; 2. Agricultural Mechanical Technology Promotion Station of Zhenjiang, Zhenjiang 212013, China). pp 73-76

Abstract: In order to explore the way to reduce energy threshold in X-shape welding formation of TC4 sheet, the influence of surfactant type, coating thickness and coating position on back reflection induced synergistic laser welding was systematically analyzed in this paper. The results show that the effect of different kinds of surfactant were different. Among them, coating NaCl and NaF is conducive to the formation of back reflection plume effects, while coating TiO_2 has some weak effect. At the same time, the back reflection plume effect was further enhanced the increase of the surfactant coating thickness NaF was more sensitive to the coating thickness than NaCl. In addition, there is little effect when coating surfactant on the back of weld. It is concluded that the effect of surfactant on the back reflection induced synergistic laser welding of TC4 sheet is mainly due to the gain of laser energy absorption.

Key words: titanium alloy sheet; laser welding; back reflection plume effect; surfactant; welding appearance

Recognition of weld seam for tailored blank laser welding based on least square support vector machine ZOU Yuanyuan[1,2], ZUO Kezhu[1,2], FANG Lingshen[3], LI Pengfei[1,2] (1. School of Mechanical Engineering, Shenyang Jianzhu University, Shenyang 110168, China; 2. National-Local Joint Engineering Laboratory of NC Machining Equipment and Technology of High-Grade Stone, Shenyang 110168, China; 3. Shenyang Institute of Automation, Chinese Academy of Sciences, Shenyang 110016, China). pp 77-81

Abstract: Accurate recognition of weld seam was the key for structural-light visual inspection of weld quality with high precision in tailored blank laser welding. Because of the problem that when the distortion of laser stripe was not obvious in the image and the welding seam cannot be recognized accurately, a recognition method according to the texture information of weld seam based on least squares support vector machine was proposed in this paper. Firstly, the textural features of the image were analysed and the textural features which had obvious difference between weld seam region and non-welded region were extracted. Secondly, the least square support vector machine model was trained and the coarse recognition of weld seam was accomplished. Finally, a fine recognition was achieved by Laws texture filter and threshold segmentation. The recognition experiments were carried out for weld seam in different welding parameters and the results showed that the weld seam can be recognized effectively by this method.

Key words: weld seam recognition; image segmentation; least square support vector machine; tailored blank laser welding

Weldability of Inconel 718 and 304 stainless steel by electron beam welding LI Ning[1,2], WANG Gang[3], WANG Ting[1,2], JIANG Siyuan[1,2], FEN Jicai[1,2,3] (1. State Key Laboratory of Advanced Welding and Joining, Harbin Institute of Technology at Weihai, Weihai 264209, China; 2. Shandong Provincial Key Laboratory of Special Welding Technology, Harbin Institute of Technology at Weihai, Weihai 264209, China; 3. State Key Laboratory of Advanced Welding and Joining, Harbin Institute of Technology, Harbin 150001, China). pp 82-85

Abstract: The electron beam welding test of Inconel 718 nickel-based superalloy and 304 stainless steel was carried out, and the microstructure and mechanical properties of the joint were analyzed. The results show that the middle of the weld zone is composed of fine equiaxed grains, and in the near-nickel side and near-steel fusion lines, there are some growth directions. The hardness of the joints is different among WZ 304 stainless and Inconel 718 and the handless of WZ is higher than that of Inconel 718 and 304 stainless steel. When the welding beam is 8 mA and the welding speed is 700 mm/min, the tensile strength of the joint is 722 MPa. Tensile studies showed that the fracture occurred at the weld zone. The